CORRECTING FOR METABOLITE CONCENTRATION DIFFERENCES BETWEEN TISSUE TYPE IN THE ADULT HUMAN BRAIN

by

AUSTIN MANNING

A THESIS

Presented to the Department of Neuroscience
and the Robert D. Clark Honors College
In partial fulfillment of the requirement for the degree of
Bachelor of Science

May 2025

An Abstract of the Thesis of

Austin Manning for the degree of Bachelor of Science
in the Department of Neuroscience to be taken May 2025

Title: Correcting for Metabolite Concentration Differences
Between Tissue Type in the Adult Human Brain

Approved: *Ian Greenhouse, Ph.D.*
Primary Thesis Advisor

Disorders of the basal ganglia have a profound impact on the motor and cognitive functions of affected individuals. Magnetic resonance spectroscopy (MRS) has increasingly been used alongside magnetic resonance imaging (MRI) to uncover the mechanisms behind such disorders by measuring molecular concentrations in the brain in vivo. One such molecule of interest is glutathione, one of the principal antioxidants in the brain, which has shown altered concentrations in the brains of individuals with basal ganglia disorders. Due to the variability in subcortical neuroanatomy between participants in MRI and MRS studies, obtaining reliable and consistent MRS measurements remains elusive. We employed brain tissue segmentation methods to account for disparities in metabolite concentration measurements, and performed analyses on segmentation results to see if subcortical tissue segmentation is consistent and specific to the regions being measured. These corrections were done to support the reproducibility and reliability of neuroimaging protocols in order to prove the efficacy of these protocols for their use in clinical applications. Our results found that subcortical tissue segmentation was consistent across multiple visits, and tissue fractions were specific to the regions being measured. Surprisingly, we found that segmentation results differed between T1- and T2-weighted MRI scans for both gray matter and white matter. These results suggest that there may be discrepancies if choosing to segment MRI scans based on how the images are weighted.

Acknowledgements

I would like to express my deepest gratitude to Professor Ian Greenhouse for his commitment, openness, and support for me as an undergraduate. By pushing me in the right direction and urging me to discover answers for myself, I have been able to better understand what it means to be a researcher and a learner, and he has allowed me to find a great passion for a subject I would've never expected coming into college. I also want to thank Professor Ellen Fitzpatrick for her guidance in the thesis prospectus writing process, and for her willingness to serve as the CHC representative on my thesis committee.

A thank you to Chris Horton for his support with the coding, data analysis, and any questions that I had surrounding this project. Without his answering my many questions in the MRI control room, I would not have gained the insight and interest in the subject that I have now. Lastly, thank you to all members of the Action Control Lab for providing a truly welcoming, informative, and enjoyable environment for me to develop as a student and as a person.

Table of Contents

Introduction

The basal ganglia are a group of nuclei situated at the base of the forebrain, involved in regulation of behavior and motor control. Its primary components include the striatum, globus pallidus (GP), subthalamic nucleus (STN), and substantia nigra (SN). Regions of the SN, including SN pars compacta (SNc) and pars reticulata (SNr) provide output from the basal ganglia to the brainstem and the thalamus, often referred to as the "relay station" of the brain. The basal ganglia pathway is organized in the "motor circuit" involving cortico-subcortical pathways that give rise to inhibitory neuronal projections that regulate the overall amount of movement. There are two basic pathways that comprise the functionality of the basal ganglia: The direct pathway, which constitutes a net excitatory motor loop, and the indirect pathway, which constitutes a net inhibitory motor loop. Both pathways involve extensive dopaminergic communication between the SN and the striatum, highlighting the role of dopamine in motor control and movement regulation. Both the direct and indirect pathways communicate further with the thalamus to route motor control with the cortex (Jankovic et al., 2021).

The SNc plays a significant role in modulation of movement as it is one of the principle producers of dopamine and dopaminergic cells in the brain, which innervate the striatum via the nigrostriatal pathway. Dopaminergic cells are largely depleted in the SNc of patients with Parkinson's disease (PD), making it a primary region of interest for movement disorders that often involve dopaminergic dysfunction (Blandini et al., 2000). Dopamine serves as a neurotransmitter between the SNc and the striatum, and if it remains non-metabolized in cellular cytosol, it may contribute to oxidative stress; that is, in the presence of oxygen, dopamine can oxidize to form neurotoxic molecules, which can then lead to the formation of reactive oxygen species (ROS), potentially impairing mitochondrial function and contributing to neuronal

damage (Bottino et al., 2021). Other potential causes of PD include prolonged exposure to environmental toxins such as pesticides, metals, and other pollutants (Goldman, 2014), but dopamine toxicity remains one of the primary hypotheses.

In response to dopamine dysfunction, glutathione (GSH) is a major antioxidant in the brain that originates from the amino acids cysteine, glutamate, and glycine, and serves to protect against ROS that cause oxidative stress damage to neurons (Asantewaa et al, 2021). High levels of ROS have been linked to cerebral tissue damage, as decreased GSH concentrations have been described in numerous basal ganglia disorders, particularly PD. The role of GSH is to reduce oxidizing reagents, producing oxidized GSH in the form of GSH disulfide (GSSG). GSSG is reduced to reform GSH, a reaction that is highly expressed in oligodendrocytes and microglia, and roughly 98 percent of GSH in the brain is in its reduced form (Rae et al., 2017). Reduced GSH acts as a redox buffer, which helps to maintain intracellular redox homeostasis, preventing harmful oxidation of various proteins. GSH can also act as a neurotransmitter, and is thought to exert dual agonistic/antagonistic effects on N-methyl-D-aspartate (NMDA) receptors, facilitating their role in synaptic plasticity (Aoyama et al., 2008).

GSH is naturally produced in the liver, where it is both synthesized and held in the cytoplasm of cells (Lu, 2013). Decreased levels of GSH in the SN have been associated with the development of PD, with numerous studies showing low levels of GSH to contribute directly to the death of dopaminergic cells in the SN, as well as that boosting GSH biosynthesis prevents age-related dopamine neuron loss (Martin et al., 2024). While literature values for GSH concentrations in the brain are highly variable, numerous studies have noted GSH levels to be approximately 2-3 mM in the brain, specifically 0.21 mM in cortical neurons (Aoyama et al., 2008), and several studies noting glial concentrations of roughly 3.8 mM (Rae et al., 2017).

Brain metabolite concentrations are quantified using proton magnetic resonance spectroscopy (MRS), which involves placement of a three-dimensional block, known as a voxel, within an anatomical image of the brain obtained using magnetic resonance imaging (MRI). Proton MRS utilizes the spin of hydrogen atoms in molecules, and applies various magnetic fields to take advantage of spatial interactions between molecules in the brain. Proton MRS combines a static magnetic field (B_0) that aligns protons in a high- or low-energy state with a radio frequency (RF) field that "excites" nuclear spins to rotate protons away from the static linear alignment to a transverse plane. The time that it takes for protons spinning in the transverse plane to go out of phase with one another is known as the T2 relaxation time, while the time it takes for protons to realign with the B_0 field is known as the T1 relaxation time, with both T1 and T2 generating contrasting images. A gradient magnetic field then encodes spatial information by adding a small component to the B_0 field, allowing for localization of the spectroscopic signal within a specific region (Buonocore et al., 2015). Both T1 and T2 differ across tissue types in the brain, which allows for the construction of anatomical images.

After the RF pulse is applied, the time that it takes for protons to move out of alignment with one another is known as the proton precession rate. Precession rates of protons differ according to the molecular structure in which they reside due to electron clouds, which can affect the magnetic field felt by the proton. Essentially, different chemical environments affect each proton's magnetic field, which can shift the precession rate. These different precession rates or "chemical shifts" are captured in the MRI scanner within a volume of interest (VOI) to generate a spectrum that reveals the relative concentrations of these molecules in parts per million (ppm). Thus, spectra that are generated with MRS are revealed to show concentrations of metabolites in proportion to the chemical environment that they reside in. Spectra are often acquired for

individual metabolites and combined or “fitted” onto a single spectrum to show relative concentration estimates.

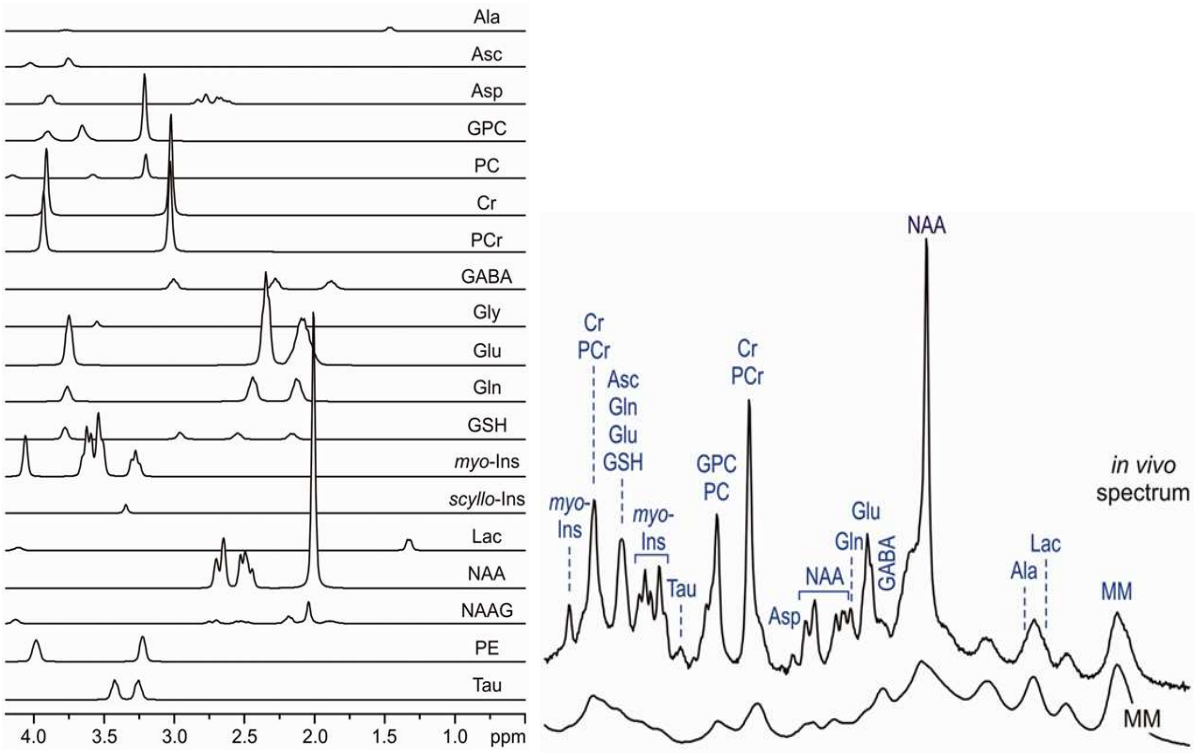

Figure 1. Spectra generated using proton MRS to reveal metabolite concentrations relative to their surrounding chemical environment. Concentrations are measured in parts per million (ppm) to reflect their chemical shift based on the electron clouds around the protons (Bottino et al., 2021).

Accurately measuring metabolite concentrations using MRS is particularly challenging in subcortical brain regions. This difficulty arises from signal interference by more superficial cortical areas and the complexity of distinguishing deeper brain tissues, which are less distinct than those near the surface. Additionally, overlapping signals from other metabolites such as aspartate, glutamate, and glutamine can further disrupt signal quality (Sanaei Nezhad et al., 2017). The primary tissues of the brain include gray matter (GM), composed mainly of cell bodies; white matter (WM), made up of neuronal axons; and cerebrospinal fluid (CSF), which

contains water, sugars, and proteins. Since metabolite concentrations vary significantly by tissue type, obtaining a clear, well-resolved signal is essential for accurately distinguishing tissues and quantifying their respective metabolite levels.

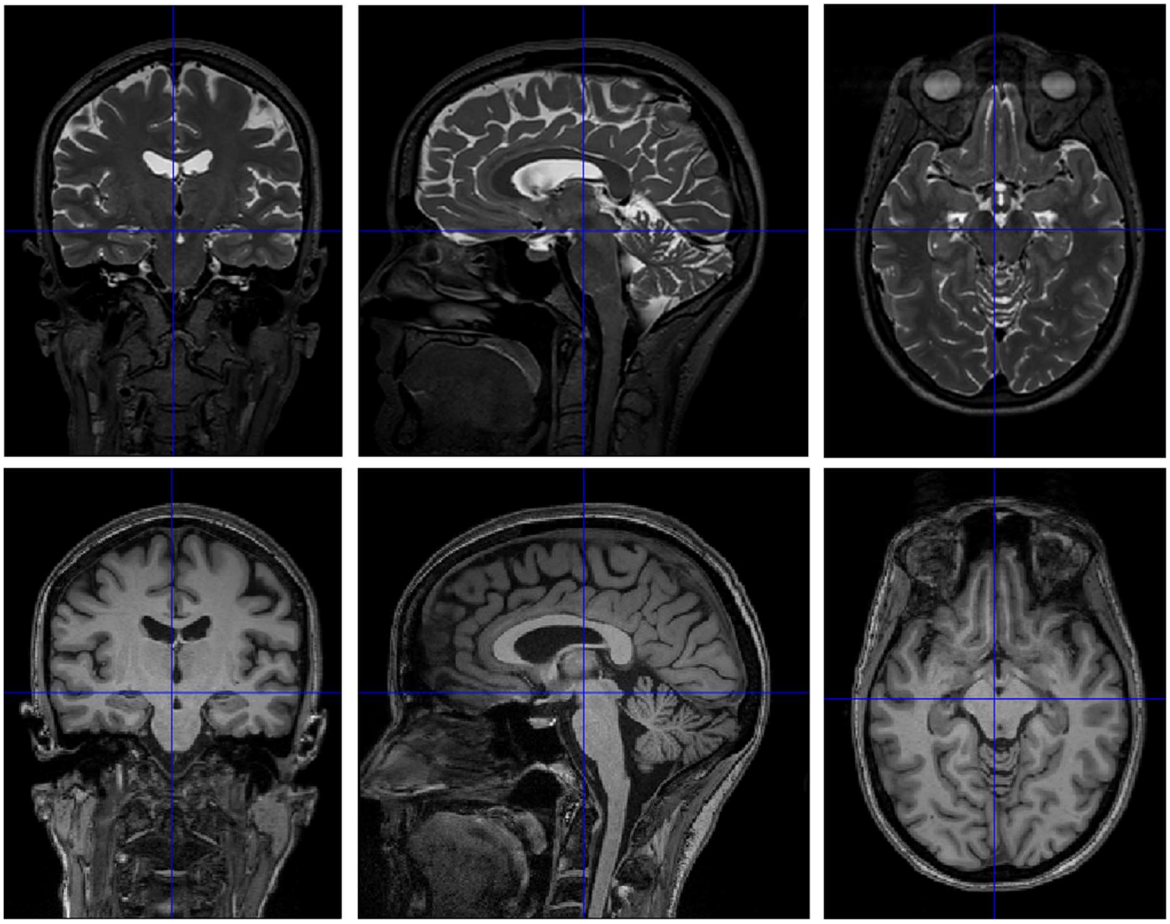

Figure 2. Comparison of T2-weighted MRI (top) with T1-weighted MRI (bottom) showing contrasting images between WM and GM. Obtained using a 3T MRI scanner (Lewis Center for Neuroimaging, University of Oregon).

While there is wide variation in the concentration of GSH between tissue types, an example study reported GSH concentrations in WM at around 1.18 mM, and concentrations in GM around 0.83 mM when measured from biopsy specimens in the monkey parietal cortex, postmortem (Aoyama et al., 2021, Slivka et al., 1987). A similar study using MRS also found levels of GSH to be 30 percent higher in WM-dominated frontal cortex compared to GM-

dominated prefrontal cortex (An et al., 2015). However, a previous study using MRS found GSH concentrations to be higher in GM (3.3 mM) than in WM (2.1 mM) when measured above the medial ventricular region (Srinivasan et al., 2010). Additionally, levels of GSH using two-photon imaging have been estimated up to three times higher in developing neurons, such as the subgranular zone of the hippocampal dentate gyrus (Sun et al., 2006). CSF is often disregarded for concentration measurements because GSH levels are deemed negligible. As such, the location of GSH in the brain is highly tissue-dependent and such wide variability in literature values stresses the need for metabolite concentration corrections.

Quantification of GSH by MRS can be done simultaneously with the neurotransmitter gamma-aminobutyric acid (GABA). MRS voxels are placed manually, requiring the researcher to differentiate between WM, GM, and CSF on the MRI scan. Because of the variation in manual voxel placements and underlying tissue composition across different participants, metabolite measurements are susceptible to variability. Thus by combining automatic tissue segmentation methods with a statistical model to correct for differences in GSH measurements based on voxel placement and the relative tissue volume it encompasses, it serves to yield a tissue-corrected concentration estimate based on within-voxel tissue fractions.

A statistical model is applied to correct for concentrational GSH differences across tissue types based on that of Harris et al., for which the technique was applied to GABA (Harris et al., 2015). This method was performed by quantifying the total GABA concentration within the voxel and rationalizing it with the relative tissue fractions of GM and WM in the voxel. GABA corrections are based on the within-voxel fraction of GM fraction, assuming it is equivalent to WM. For the correction of data in human subjects, an arbitrary unit termed "α" is used to represent an assumed ratio between metabolite concentrations in GM and WM. Because the

amount of GABA in CSF is negligible, it was not included in this model. Because this statistical method was successful with rationalizing GABA, it is supported for quantifying other metabolites, including GSH.

When conducting MRS, metabolite concentrations are calculated in arbitrary institutional units. Because the volume of water per unit is well known for different tissue types in the brain, the strong signal that water produces can be used as a reference for other metabolites with respect to their concentration, a method adopted from Gasparovic et al. This method is based on the signal from water within the voxel being proportional to the number of moles of the molecule in the voxel. Volume fractions of GM, WM, and CSF are determined by segmentation, and molal water concentration is measured to relate tissue volume fractions to relative water fraction in each segmentation. The molal water concentration (moles/kg of solvent) of MR-visible water in the metabolite solution is assumed to be that of pure water (55.51 mol/kg) to quantify metabolite concentration within the voxel (Gasparovic et al., 2006). An alternative reference molecule, Creatine (Cr), is also often used to quantify metabolite concentrations because of its spectral resonance peak at 3.00 ppm, which is a similar resonance frequency to that of GABA (3.00 ppm) and GSH (2.95 ppm).

Tissue segmentation is a common method to identify the fraction of tissue type within voxels. Using Statistical Parametric Mapping software (SPM), segmentation is performed using tissue probability maps, assigning each voxel a probability of belonging to each tissue type, which is done by using shading thresholds to discriminate between the probability of a region being GM, WM, or CSF (SPM12, University College London, 2014). SPM uses the DARTEL and CAT12 toolboxes, which aid in both shaping and filling images. Due to the difficulty of accurately measuring subcortical metabolite concentrations, cortical tissue segmentation is used

as a control for the various within-voxel tissue fractions. A 2016 study using SPM8 software reported percentages of GM, WM, and CSF in the anterior cingulate cortex at 41.9, 50.8, and 7.3, and in the occipital cortex, percentages were reported at 59.0, 28.7, and 12.3, respectively (Sanaei Nezhad et al., 2017). These values serve as references for subcortical segmentation.

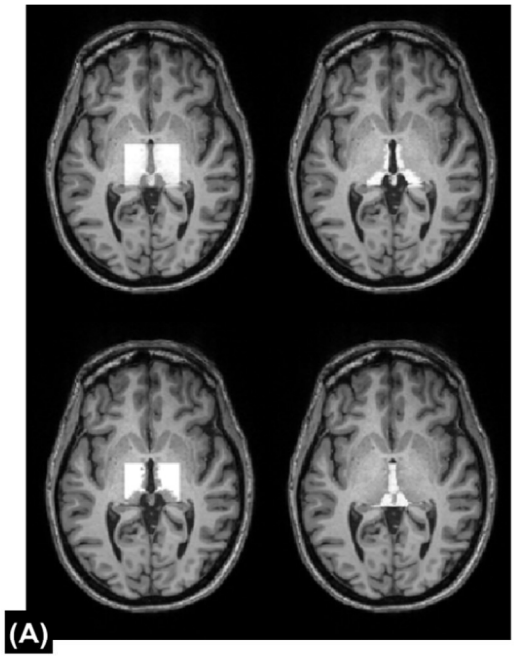

(A)

Relaxation-, tissue-corrected (Gasparovic et al. method)

GABA+/Water: 4.61 i.u.

Glx/Water: 10.69 i.u.

GSH/Water: 1.50 i.u.

Relaxation-, tissue-, alpha-corrected (Harris et al. method)

GABA+/Water: 4.73 i.u.

Glx/Water: 10.97 i.u.

GSH/Water: 1.54 i.u.

Relaxation-, tissue-, alpha-corrected; average-voxel-normalized (Harris et al. method)

GABA+/Water: 3.21 i.u.

Glx/Water: 7.45 i.u.

GSH/Water: 1.05 i.u.

(C)

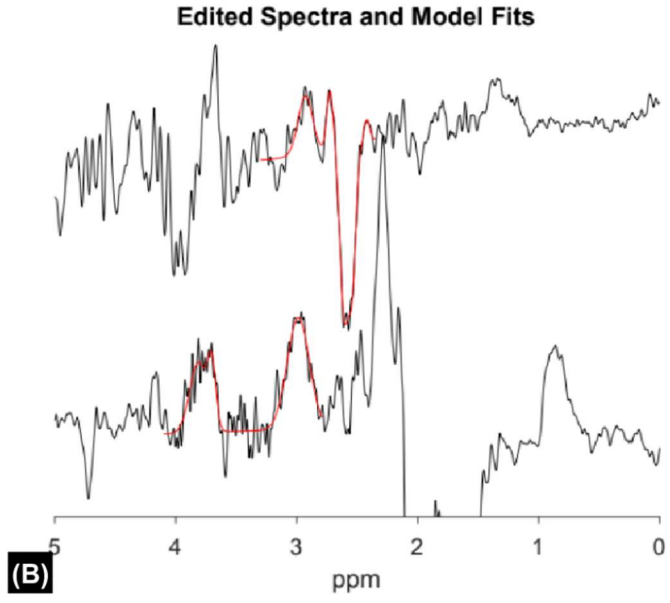

(B)

Figure 3. (A) Subcortical tissue segmentation using SPM12 shows the substantia nigra VOI on a T1-weighted MRI of an individual participant. The figure shows the entire voxel (top left), the segmented fraction of GM (top right), WM (bottom left), and CSF (bottom right). **(B)** Models were fit to the spectra edited for GSH and GABA using Gannet software for metabolite estimation.. The top line in red shows the model fit to the GSH peak around 2.95 ppm, and the bottom line in red shows the model fit to the GABA peak around 3.00 ppm. **(C)** Concentration measurements of GSH and GABA were estimated using the correction-quantification methods discussed.

Methods

The long term goal of the current lab project is to develop an MRI protocol with sensitivity to Parkinson pathology. The project focuses on establishing a neuroimaging protocol that is reliable with regional specificity, to lay groundwork for clinical PD research with healthy older adults.

For this study, it was important to ensure that metabolite measurements were specific to the regions being measured (thalamus and SN). By building off of the previously mentioned statistical model that corrects for differences in GSH (and overall metabolite) concentrations, the project aims to support the reliability and precision of measurements obtained using new neuroimaging protocols. The participants included 11 healthy older adults aged 50 to 80 years (57.8 ± 8.0 years) with no neuropsychiatric disorders, for which cognitive analysis was conducted using the Mini Mental State Examination (MMSE). It was expected that this sample of subjects closely resembled the population of individuals susceptible to PD to allow for applicability of the study to the broader population.

Using a 3T Siemens Prisma MRI scanner (Lewis Center for Neuroimaging, University of Oregon) with a 32-channel head coil, participants were subjected to two MRI scans, roughly 14 days apart at the same time of day to control for the diurnal variation in metabolite

concentrations. Subjects were placed into the scanner headfirst in supine position. For each scan, a high-resolution T2-weighted whole brain sagittal MRI (TR = 3200 ms; TE = 408 ms; 230 × 230 mm in plane, 0.9 mm slice in thickness, 5:03 min total acquisition time, iPAT acceleration factor of 2) and high-resolution T1-weighted whole brain sagittal MRI (TS = 2500 ms; TE = 3.43 ms; 256 × 256 mm in plane, 1 mm slice thickness, 4:15 min total acquisition time, iPAT acceleration factor of 2) was acquired for MRS voxel placement. The anatomical images taken from these MRI scans were used to guide the manual positioning of the MRS VOIs that were placed bilaterally in the left and right thalamus, as well as SN. In this study, voxels consisted of a VOI in the SN (40 × 30 × 20 mm^3) and the left and right thalamus (each 25 × 30 × 25 mm^3) capturing GM, WM, and CSF.

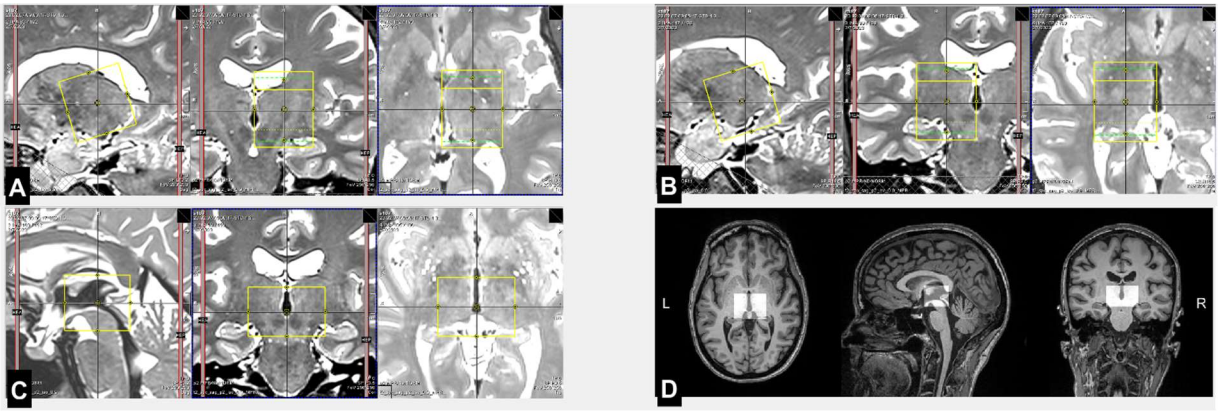

Figure 4. VOI three-dimensional voxel placement in structural MRI. Planes in each panel from left to right are sagittal, coronal, and transverse. Voxels shown are the left thalamus **(A)**, right thalamus **(B)**, substantia nigra **(C)**, and T1-weighted whole-brain MRI with the VOI in the substantia nigra **(D)**.

Following manual voxel placement, single-voxel proton MRS was performed to measure chemical content in the target VOI. As metabolites were measured, they produced a peak on the magnetic resonance spectrum where the spectral position corresponded to the specific proton resonance frequency, and spectral height corresponded to the number of proton signals at that

frequency; GSH exists at around 2.95 ppm on the MR spectrum. The specific project protocol used measurements of GABA, GSH, water, and Cr, where water and Cr are used as reference signals because the peak area of both metabolites is relative to the ratio of the GSH and GABA peak area. Water is a useful reference because of its prevalence and known molarity in the brain, but the Cr peak around 3.00 ppm on the MR spectrum is used as an additional reference because of its similar resonance frequency to GABA and GSH. Because of the presence of numerous metabolite signals in a sample, they often obscure one another's observable signal. Thus, the Hadamard Encoding and Reconstruction of MEGA-edited Spectroscopy (HERMES) pulse sequence was used to separate molecules on the observable spectrum.

The HERMES editing scheme used in this project utilizes an editing technique known as J-difference editing, which resolves signals that obscure GSH and GABA peaks (Chan et al., 2016). This technique is based on two sets of sub-scans, involving an ON scan in which frequency-specific pulses are applied to the spins of GSH protons, and an OFF scan in which these pulses are not applied. The ON and OFF scans are subtracted to reveal a "difference-edited" spectrum that removes the signals of metabolites that are unaffected by the editing pulse, allowing visualization of the GSH signal on a spectrum. By utilizing J-difference editing, the shape of the GSH signal is different in the ON and OFF cases, whereas overlying Cr signals remain the same, so that subtraction of the ON and OFF cases removes the Cr signal while revealing the observable GSH signal. In this study, the HERMES sequence parameters were matched to previously published studies (TR = 2000 ms; TE = 80 ms; 90 degree flip angle, 4 prep scans, 160 averages; GABA edit pulse frequency = 1.9 ppm; GSH edit pulse frequency = 4.56 ppm; Off-frequency edit pulse = 7.5 ppm; weak water suppression = 50 Hz). These parameters were the same across all three VOIs.

MRS data was processed and analyzed using the Gannet toolkit in MATLAB, which takes raw data input and processes it to generate edited spectra, applying a modeling procedure that estimates GABA and GSH concentration with respect to the Cr signal or water signal (Edden et al., 2014, Mikkelsen et al., 2016). The three main Gannet functions utilized were GannetLoad, GannetFit, and GannetCoRegister. The GannetLoad function imports time-domain data from the scanner and processes it into a frequency domain metabolite-edited spectrum, and the GannetFit function integrates edited metabolite peaks at their respective ppm and reproduces metabolite concentration estimates. The GannetCoRegister function combines VOIs with the segmented anatomical images, yielding the fraction of tissue type within each VOI. Corrections for GABA that have been performed by Harris et al. are embedded in the Gannet code. Corrections for GSH exist here as well, but it remains a rough estimate of the GSH concentrations in gray and white matter, noting the ratio at 1:1 for GM and WM.

In order to differentiate between brain tissue type on anatomical MRIs, SPM software was used as a basis for segmenting within-voxel GM, WM, and CSF fractions using classifications of tissue type (SPM12, University College London, 2014). Using tissue probability maps, the volume of each tissue classification was set at threshold levels of 0.5, 0.8, and 0.9, each generating a different binary mask for tissue probability. In other words, depending on the magnitude of lightness or darkness in the shading of the VOI, SPM determined the likelihood that that region fell above or below the tissue threshold on a scale between 0.0 and 1.0. The volume for each tissue class and threshold pair was obtained by multiplying the number of voxels with an assigned probability above a given threshold with the dimension of the voxel.

Statistical data was analyzed in JASP using four-way repeated measures ANOVA and post hoc comparisons (JASP version 0.19.3, 2024). The repeated measures factors included scan

type (T1 or T2), visit number (first or second visit), VOI location (right thalamus, left thalamus, or SN), and tissue type (GM, WM, or CSF). Significant interactions were followed up with post hoc comparisons to evaluate the extent to which these interactions were relevant. Fractional tissue values from GannetCoRegister were input in the repeated measures cells to assess the effects of all four variables on the consistency of the data. By comparing descriptives of data in JASP to those of cortical tissue fractions as controls, the reliability and reproducibility of the measurements obtained could be rationalized.

Results

Four-way repeated measures ANOVA in JASP showed that mean fractional tissue composition between voxels differed significantly: right thalamus (0.26 ± 0.03 GM; 0.62 ± 0.03 WM; 0.12 ± 0.03 CSF), left thalamus (0.25 ± 0.04 GM; 0.61 ± 0.06 WM; 0.14 ± 0.05 CSF), and SN (0.25 ± 0.04 GM; 0.55 ± 0.05 WM; 0.20 ± 0.06 CSF). Each participant yielded 36 data points (T1-T2 × visit × voxel × tissue) for a total of 396 data points. Data for the T2 scan of the second visit for participant s187 was not included, nor was data for T1 scan for the first visit of participant s242. These missing data points were replaced with the data acquired from the participant's other scan.

Main Effects

There was a significant main effect of tissue type, $F(2,20) = 361.68$, $p < .001$, indicating that the proportion of GM, WM, and CSF differed significantly across conditions including VOI and scan type. No significant effects were found for scan type (T1 or T2): $F(1,10) = 1.06$, $p = .33$, for visit number (visit 1 or visit 2): $F(1,10) = 1.20$, $p = .30$, or for voxel location: $F(2,20) =$

0.83, p = .45. These results suggest that measurements were consistent across visits and scan types, and voxel location did not have a significant influence on overall tissue fraction estimates.

Two-Way and Higher-Order Interactions

A significant voxel × tissue interaction was observed, $F(4,40) = 14.03$, $p < .001$, indicating that tissue composition varied depending on voxel location, which was in-line with our predictions. WM fractions were highest in thalamic voxels compared to the SN, where GM was more concentrated. A significant interaction was also found between T1-T2 × tissue, $F(2,20) = 21.66$, $p < .001$, indicating that tissue classification differed across scan types. There were no other significant two-way interactions, nor were there significant three-way or four-way interactions. This includes visit × tissue, $F(2,20) = 0.071$, $p = 0.93$, for which the absence of a significant effect indicates that fractional tissue measurements did not differ across visits. The lack of higher-order interactions suggests that tissue fraction consistency was not reliant on any specific combinations of scan parameters.

Post Hoc Comparisons

Given the significant interaction between tissue type and scan type from the ANOVA, post hoc comparisons were performed. Post hoc found that for GM, the proportion of tissue was significantly higher in T1 scans compared to T2 scans, $t(10) = 6.105$, $p < .001$, Cohen's $d = 1.141$. WM showed a pattern comprising a significantly higher proportion in T2 scans compared to T1, $t(10) = -3.804$, $p = .003$, $d = -0.814$. CSF also differed significantly between scan types, showing lower values in T1 scans, $t(10) = -2.680$, $p = .023$, $d = -0.328$.

Figure 5. Plots showing tissue fractions within voxels between T1- and T2-weighted MRI across two visits. T1-weighted images had a higher estimation of GM within all voxels (left) while T2-weighted images had a higher

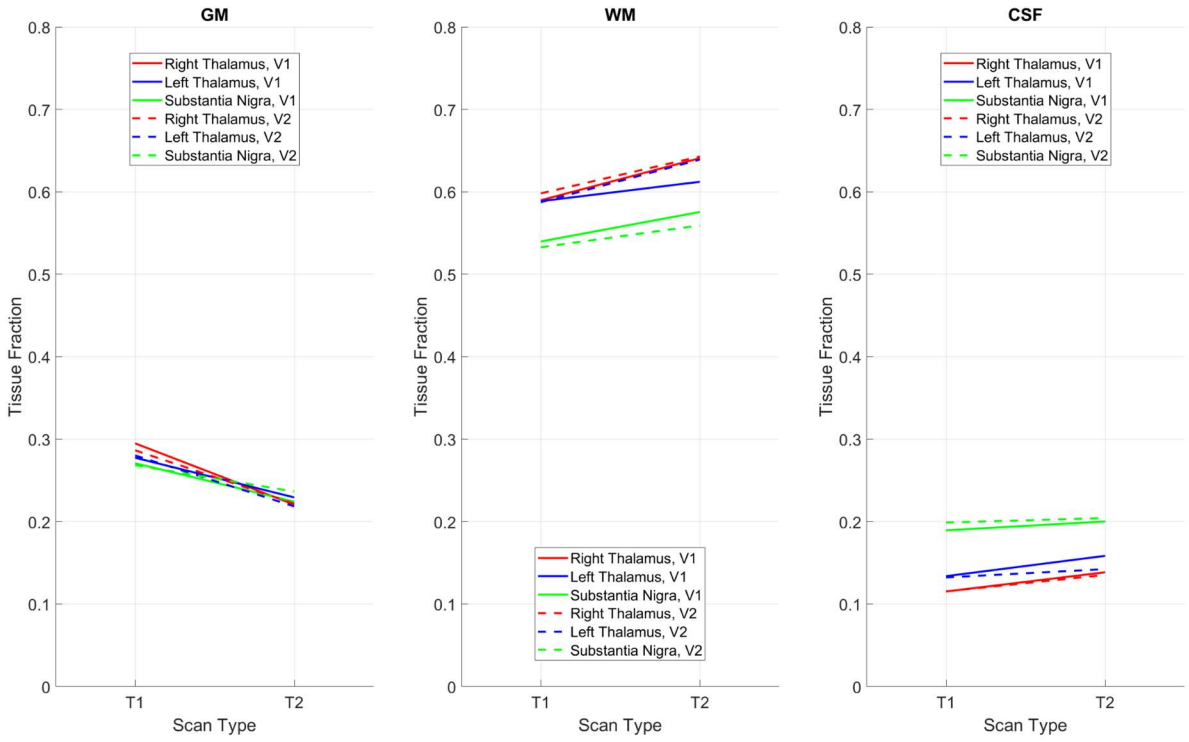

estimation of WM within all voxels (middle). T2-weighted images also had a slightly higher estimation of CSF within voxels, but not to a significant degree (right).

Descriptive Statistics

Descriptives (Table 1) confirmed high reproducibility across visits and scan types. Mean tissue fractions across all VOIs and tissues were consistent with low standard deviations. Coefficients of variation were below 10 percent for most WM values and slightly higher for CSF, which is more susceptible to segmentation variation due to its smaller prevalence in the study VOIs.

Table 1. Descriptive statistics in JASP revealed mean tissue fraction (GM, WM, CSF) within each VOI (RThal,

T1-T2	Visit	Voxel	Tissue	N	Mean	SD	SE	Coefficient of variation
T1	Visit1	RThal	GM	11	0.295	0.016	0.005	0.054
			WM	11	0.590	0.030	0.009	0.051
			CSF	11	0.115	0.035	0.010	0.300
		LThal	GM	11	0.278	0.029	0.009	0.103
			WM	11	0.589	0.037	0.011	0.063
			CSF	11	0.134	0.051	0.015	0.382
		SN	GM	11	0.271	0.035	0.010	0.128
			WM	11	0.540	0.042	0.013	0.077
			CSF	11	0.189	0.069	0.021	0.362
	Visit2	RThal	GM	11	0.287	0.029	0.009	0.102
			WM	11	0.598	0.023	0.007	0.039
			CSF	11	0.115	0.036	0.011	0.309
		LThal	GM	11	0.280	0.039	0.012	0.138
			WM	11	0.587	0.032	0.010	0.054
			CSF	11	0.132	0.043	0.013	0.325
		SN	GM	11	0.268	0.033	0.010	0.124
			WM	11	0.533	0.040	0.012	0.074
			CSF	11	0.199	0.064	0.019	0.324
T2	Visit1	RThal	GM	11	0.221	0.039	0.012	0.176
			WM	11	0.641	0.046	0.014	0.071
			CSF	11	0.139	0.029	0.009	0.211
		LThal	GM	11	0.229	0.063	0.019	0.275
			WM	11	0.612	0.126	0.038	0.206
			CSF	11	0.158	0.079	0.024	0.496
		SN	GM	11	0.224	0.047	0.014	0.208
			WM	11	0.576	0.041	0.012	0.071
			CSF	11	0.200	0.062	0.019	0.312
	Visit2	RThal	GM	11	0.222	0.043	0.013	0.195
			WM	11	0.643	0.039	0.012	0.061
			CSF	11	0.135	0.032	0.010	0.235
		LThal	GM	11	0.219	0.039	0.012	0.177
			WM	11	0.639	0.033	0.010	0.052
			CSF	11	0.142	0.038	0.011	0.264
		SN	GM	11	0.237	0.055	0.017	0.233
			WM	11	0.559	0.040	0.012	0.072
			CSF	11	0.204	0.048	0.014	0.235

LThal, SN) respective of scan type (T1-T2) and visit number (visit 1 and visit 2).

Discussion

It was expected that segmentation would show significant differences between tissue type and voxel position within subcortical brain regions, and that measurements would be consistent across visits. Tissue segmentation with SPM12 showed accurate and consistent results when comparing fractions of GM, WM, and CSF within the VOIs in this study, with significant voxel × tissue interactions. The lack of significant interactions between visit × tissue indicates that measures were not only consistent across visits, but manual voxel placement was also reliable for

given regions. This supports the efficacy of the use of SPM12 software for subcortical tissue segmentation using proton MRS, as well as the reliability that placing subcortical voxels manually can yield reproducible results. Given the consistency of our segmentation methods, it is promising for the use of such methods in clinical applications, as reproducible imaging and analysis methods are essential in understanding basal ganglia disorders, and neurological disorders in general. For longitudinal studies, reliable segmentation also ensures that changes observed over time accurately reflect anatomical and pathological changes when combined with MRS, rather than variability in voxel placement.

An unexpected finding of the study was that of the significant difference between T1 and T2 scan estimates of WM and GM within voxels. Table 1 shows that a slightly higher amount of WM across all VOIs was estimated using T2 scans as compared to T1 scans. T1 scans showed the opposite relationship, in which GM was seen to make up a larger tissue fraction within voxels as compared to T2 scans. This could largely be due to how the SPM probability mapping differentiates shading gradients between T1- and T2-weighted images. When deciding between the two, T2-weighted images may be better for use in subcortical segmentation because of its highlighting of differences in water content. This allows for a higher contrast between tissue type, improved visibility of smaller nuclei, and a clearer delineation of CSF spaces as CSF is much brighter on T2-weighted images. However, future studies that employ segmentation methods could achieve the most reliable results by combining both T1 and T2 scans to compensate for how the two differ in whole-brain and subcortical segmentation, as well as combine anatomical detail. The differences in T1- and T2-weighted image segmentation also highlight the difficulty in measuring metabolite concentrations in subcortical brain regions.

The results of this study are in agreement with other studies showing the reliability of SPM12 segmentation in cortical structures (Sanaei Nezhad et al., 2017, Harris et al., 2015). Because there are limited studies utilizing tissue segmentation in subcortical structures, this study is both intriguing and promising by means of exploring segmentation in VOIs that include the SN and thalamus. As mentioned in the introduction, the existing literature varies largely in how GSH concentrations are estimated between GM and WM. While the results of this study showed that subcortical tissue segmentation is reliable, there is still much to be done in the quantification of metabolite concentrations relative to tissue type, and how these change with neuroanatomy over time.

An extension of this study could be to further consider the effects of cell type on metabolite concentration differences in the brain. While this has been done in limited capacity, it could serve to support or reject the results of this study given that GM, WM, and CSF are made up of widely different types of cells. For example, a study using two-photon imaging found increased GSH levels in lateral ventricle ependymal and meningeal cells at the blood-brain interface and lining the ventricles, which is important to consider given the role that cell type plays in tissue differentiation (Rae et al., 2017). This is beneficial to note, considering if voxels in MRS studies include ventricular and meningeal regions. While it would not be possible to parse out cell type based on tissue segmentation alone, the combination of tissue differentiation with MRS protocols and cell differentiation could reveal much about subcortical metabolite mechanisms, including that of GSH. Additionally, because metabolite concentrations are often disregarded in CSF, studies have suggested the possibility of calculating GSH levels in CSF from blood samples (Samuelsson et al., 2011). By combining blood sampling with MRS measurements, it could serve as an all-encompassing method of metabolite measurements.

The fact that data was collected from only eleven participants is a limitation of this study. Such a low statistical power may mean that results were more influenced by chance, and that results were less reliable. Additionally, the small sample size was more susceptible to selection bias, and may not be able to generalize to the broader population and entirely represent that of individuals susceptible to PD. Another consideration is that water tends to decrease in GM with age (Emir et al., 2011). Given the mean age of the participants in this study (57.8 ± 8.0 years), the correction method based off of Gasparovic et al. using the known water concentration could lead to overestimations of metabolite concentrations. Lastly, considering that some of the data points for participants s187 and s242 were reused, it likely resulted in an overestimation of the consistency of SPM for tissue segmentation.

In summary, our results showed that subcortical tissue segmentation using SPM12 is both reliable and specific to the regions being studied. By combining within-voxel tissue fractions with relative metabolite concentrations, correction methods can be applied to account for variations in the anatomy between subjects, which can significantly improve our confidence for implementing these methods in clinical applications. Additionally, the differences in GM and WM fraction estimations based on T1- and T2-weighted MRI revealed surprising and intriguing results that support the importance of combining these image types in real-world applications to achieve accurate results. With these findings, it is hopeful that subcortical tissue segmentation and metabolite measurements may not be as elusive as it seems, and by combining modern quantification techniques it is both promising and exciting for the future of MRS research in academic and clinical applications.

References

An, L., Li, S., Murdoch, J. B., Araneta, M. F., Johnson, C., & Shen, J. (2015). Detection of glutamate, glutamine, and glutathione by radiofrequency suppression and echo time optimization at 7 tesla. *Magnetic resonance in medicine*, *73*(2), 451-458.

Aoyama, K., Watabe, M., & Nakaki, T. (2008). Regulation of neuronal glutathione synthesis. *Journal of pharmacological sciences*, *108*(3), 227-238.

Aoyama, K. (2021). Glutathione in the Brain. *International journal of molecular sciences*, *22*(9), 5010.

Asantewaa, G., & Harris, I. S. (2021). Glutathione and its precursors in cancer. *Current opinion in biotechnology*, *68*, 292-299.

Blandini, F., Nappi, G., Tassorelli, C., & Martignoni, E. (2000). Functional changes of the basal ganglia circuitry in Parkinson's disease. *Progress in neurobiology*, *62*(1), 63-88.

Bottino, F., Lucignani, M., Napolitano, A., Dellepiane, F., Visconti, E., Rossi Espagnet, M. C., & Pasquini, L. (2021). In vivo brain GSH: MRS methods and clinical applications. *Antioxidants*, *10*(9), 1407.

Buonocore, M. H., & Maddock, R. J. (2015). Magnetic resonance spectroscopy of the brain: a review of physical principles and technical methods. *Reviews in the Neurosciences*, *26*(6), 609-632.

Chan, K. L., Puts, N. A., Schär, M., Barker, P. B., & Edden, R. A. (2016). HERMES: Hadamard encoding and reconstruction of MEGA-edited spectroscopy. *Magnetic resonance in medicine*, *76*(1), 11-19.

Coleman, C. R., Pallos, J., Arreola-Bustos, A., Wang, L., Raftery, D., Promislow, D. E., & Martin, I. (2024). Natural variation in age-related dopamine neuron degeneration is glutathione dependent and linked to life span. *Proceedings of the National Academy of Sciences*, *121*(42), e2403450121.

Detcheverry, F., Senthil, S., Narayanan, S., & Badhwar, A. (2023). Changes in levels of the antioxidant glutathione in brain and blood across the age span of healthy adults: A systematic review. *NeuroImage: Clinical*, *40*, 103503.

Dringen, R. (2000). Metabolism and functions of glutathione in brain. *Progress in neurobiology*, *62*(6), 649-671.

Edden, R. A., Puts, N. A., Harris, A. D., Barker, P. B., & Evans, C. J. (2014). Gannet: A batch-processing tool for the quantitative analysis of gamma-aminobutyric acid–edited MR spectroscopy spectra. *Journal of magnetic resonance imaging*, *40*(6), 1445-1452.

Emir, U. E., Raatz, S., McPherson, S., Hodges, J. S., Torkelson, C., Tawfik, P., ... & Terpstra, M. (2011). Noninvasive quantification of ascorbate and glutathione concentration in the elderly human brain. *NMR in Biomedicine*, *24*(7), 888-894.

Gasparovic, C., Song, T., Devier, D., Bockholt, H. J., Caprihan, A., Mullins, P. G., ... & Morrison, L. A. (2006). Use of tissue water as a concentration reference for proton spectroscopic imaging. *Magnetic Resonance in Medicine: An Official Journal of the International Society for Magnetic Resonance in Medicine*, *55*(6), 1219-1226.

Goldman, S. M. (2014). Environmental toxins and Parkinson's disease. *Annual review of pharmacology and toxicology*, *54*(1), 141-164.

Harris, A. D., Puts, N. A., & Edden, R. A. (2015). Tissue correction for GABA-edited MRS: Considerations of voxel composition, tissue segmentation, and tissue relaxations. *Journal of magnetic resonance imaging*, *42*(5), 1431-1440.

Jankovic, J., & Mazziotta, J. C. (2021). *Principles and practice of movement disorders* (3rd ed.). Elsevier.

JASP Team. (2024). *JASP (Version 0.19.3)* [Computer software]. https://jasp-stats.org/

Lu, S. C. (2013). Glutathione synthesis. Biochimica et Biophysica Acta (BBA)-General Subjects, 1830(5), 3143-3153.

MathWorks. (2024). *MATLAB (Version R2024a)* [Computer software]. https://www.mathworks.com/products/matlab.html

Rae, C. D., & Williams, S. R. (2017). Glutathione in the human brain: Review of its roles and measurement by magnetic resonance spectroscopy. *Analytical biochemistry*, *529*, 127-143.

Saleh, M. G., Oeltzschner, G., Chan, K. L., Puts, N. A., Mikkelsen, M., Schär, M., ... & Edden, R. A. (2016). Simultaneous edited MRS of GABA and glutathione. *Neuroimage*, *142*, 576-582.

Samuelsson, M., Vainikka, L., & Öllinger, K. (2011). Glutathione in the blood and cerebrospinal fluid: A study in healthy male volunteers. *Neuropeptides*, *45*(4), 287-292.

Sanaei Nezhad, F., Anton, A., Parkes, L. M., Deakin, B., & Williams, S. R. (2017). Quantification of glutathione in the human brain by MR spectroscopy at 3 Tesla: Comparison of PRESS and MEGA-PRESS. *Magnetic resonance in medicine*, *78*(4), 1257-1266.

Slivka, A., Spina, M. B., & Cohen, G. (1987). Reduced and oxidized glutathione in human and monkey brain. *Neuroscience letters*, *74*(1), 112-118.

Srinivasan, R., Ratiney, H., Hammond-Rosenbluth, K. E., Pelletier, D., & Nelson, S. J. (2010). MR spectroscopic imaging of glutathione in the white and gray matter at 7 T with an application to multiple sclerosis. *Magnetic resonance imaging*, *28*(2), 163-170.

Sun, X., Shih, A. Y., Johannssen, H. C., Erb, H., Li, P., & Murphy, T. H. (2006). Two-photon imaging of glutathione levels in intact brain indicates enhanced redox buffering in developing neurons and cells at the cerebrospinal fluid and blood-brain interface. *Journal of Biological Chemistry*, *281*(25), 17420-17431.

Wellcome Centre for Human Neuroimaging. (2024). *SPM12 (Version 7771)* [Computer software]. University College London. https://www.fil.ion.ucl.uk/spm/